

The relevance of analytical formulations predicting stiffener tripping

Jack Reijmers^{a,1}, Pieter Nobel^a

^aNevesbu B.V., Kelvinring 48, 2952 BG Alblasterdam, The Netherlands

Abstract

In search for the governing failure mode of externally pressurized ring-stiffened cylinders the focus is, due to its loading and slender geometry, drawn to elastic buckling. However, the hydrostatic pressure loading and imperfections cause nonlinear behaviour, and excessive deformation results in plastic failure, denoted by collapse. This implies that a true bifurcation point is often hardly observed, and this raises the question whether it is worthwhile to spend much effort to determine the elastic buckling pressures other than to ensure they are well above the collapse pressure? This paper focuses on the elastic buckling of ring frames, generally referred to as frame tripping. Some latest attempts in improving the accuracy of the analytical formulations will be questioned.

Firstly, this study will compare non-linear buckling with linear-elastic material behaviour to elastic buckling by means of finite element analysis. Secondly, the non-linear elastic-plastic effects will be included too. Doing so, the effect of the geometrical non-linearity and material elastic-plastic non-linearity will be visible separately and will give an indication of the relevance of frame tripping results predicted by analytical elastic buckling formulations.

Literature offers a variety on analytical formulations, each with an underlying idea to remove undesired assumptions that impair results. Even recently comprehensive formulations are published to establish an accurate value of the elastic tripping pressures.

This paper shows whether those methods are still relevant in modern pressure hull design or not.

Keywords

Ring-stiffened cylinders, Stiffener tripping, Stiffener tilt, Analytical solution, Nonlinear Finite Element Analysis.

© 2024 The Authors. Published by NAFEMS Ltd.

This work is licensed under a Creative Commons Attribution-NonCommercial-NoDerivatives 4.0 International License.

Peer-review under responsibility of the NAFEMS EMAS Editorial Team.



1 Introduction

The loading of externally pressurized submarine pressure hulls gives rise to interaction between plastic failure and elastic buckling. Stocky geometries will fail by plastic behaviour. Under hydrostatic pressure the structure shows almost linear response until the material becomes nonlinear. Slender geometries will fail by buckling. The perfect geometry will show a moderate, linear response till a bifurcation point. After reaching the bifurcation point the response suddenly becomes excessive due to the transition into the buckling mode. Introducing an imperfection, the response will demonstrate a gradual transition into the post-buckling phase depending on the severity of the imperfection. According to Koiter post-buckling behaviour can have a stable character which implies a static equilibrium for loads in excess of the buckling load. In some cases (in particular shells) the post-buckling behaviour will not be stable, and a limit point is found before the load reaches the bifurcation point [1], [2]. It must be noted that for both cases the imperfection is responsible for an asymptotic behaviour that is not linked to the elastic buckling load of perfect geometries.

¹Corresponding author.

E-mail address: j.j.reijmers@nevesbu.com (J. Reijmers)
<https://doi.org/10.59972/bcxbuxm0>

In analytical methods, for instance [3] it is common to cover this non-linearity by introducing an asymptote defined by the elastic buckling load. This gives a neutral post-buckling behaviour in which the deformation increases dramatically if the pressure tends to the bifurcation point.

Submarine pressure hulls are dwelling between slender and stocky with imperfections due to the manufacturing process. This means nonlinear response with a cut-off by plastic behaviour of the material. If the linear elastic buckling pressure is much higher than the pressure causing yield, then the nonlinearity will be small. The question is whether collapse of the pressure hull is driven by the material property, namely the yield stress or by the elastic buckling pressure. Furthermore, if the response is limited by yielding in the early phases of the pre-buckling path how large will be the nonlinear-buckling contribution? This suggests the need for an adequate method to calculate the buckling pressure and the influence of imperfections on the deformation path.

For ring-stiffened cylinders three buckling pressures are relevant. These are buckling of the shell between the ring frames (interframe buckling), buckling of the ring frames (global buckling) and rotational buckling of the frames (frame tripping).

The past century has shown a large number of papers on buckling pressures that are frequently cited. For interframe buckling the standard was set about hundred years ago by von Mises [4], [5]. With respect to global or overall buckling classification societies refer mostly to Bryant [6]. Further development of the analytical formulation of global buckling was presented by Kendrick [3]. The topic of frame tripping was addressed by Wenk & Kennard [7], Kennard [8], Kendrick [3] and Faulkner [9]. Most recently Shiomitsu & Yanagihara [10], [11] presented an extensive derivation of the analytical solution for frame tripping.

In the last decades the application of nonlinear FE analysis has grown enormously, and the role of analytical formulations shifted more and more to the background. However, when material as well as geometrical nonlinearity is considered the influence of the buckling pressure on excessive deformation is shrouded. Nevertheless, the question remains whether a linear elastic buckling pressure could be responsible for a strong nonlinear magnification in the elastic regime. If this is not the case, is it still worthwhile to put much effort in establishing eigenvalues?

This paper addresses a particular pressure hull design named Manatee class presented earlier [12], [13]. Excessive behaviour towards elastic buckling pressures is emphasized by the application of linear elastic material. By eliminating plastic behaviour, the response to increasing pressure grows geometrical nonlinear towards a possible elastic buckling pressure. Therefore, attention is paid to the establishment of these buckling pressures and associated stresses by analytical as well as numerical formulations.

It is found that there is a considerable gap between buckling pressures following from both methods, while also the predicted stresses in the ultimate fibre of the stiffener flange differ. Moreover, excessive nonlinear response cannot always be linked to a specific linear elastic buckling pressure.

This paper has a strong focus on stiffener tripping, since there is no simple and accurate formula available. In general stiffener tripping is easy to avoid with guidance regarding the geometry of web plate and flange. An example is given by Germanischer Lloyd [14] by their rules for classification and construction. Resistance against tripping can be realized with minimum weight impact and a small effect on nonlinearity in the elastic-plastic regime is anticipated. Therefore, much effort to establish accurate buckling / tripping pressures does not seem justified.

Section 2 and 3 of this paper present the theoretical background of nonlinear behaviour. The FE analyses of the buckling pressures and geometrical nonlinear behaviour follows in Section 4. Section 5 elaborates on the effect of material nonlinearity on the influence of elastic buckling pressures regarding nonlinearity. Section 6 shows the comparison between theory and numerical simulation. Conclusions and recommendations can be found in Section 7.

2 The buckling phenomenon

For explanatory purposes the well-known buckling results of a slender beam will be discussed. The familiar deformation behaviour and failure modes are of course less complex than for a submarine pressure hull. However, it is well suitable for introducing the assessment of a design formulation incorporating buckling and the effects of imperfections.

Figure 1 presents a slender tube of elastic material, pinned at the bottom and roller-supported at the top, subjected to a gradually increasing vertical compressive load. Due to the loading the slender beam

will enter its fundamental deformation mode, which is shortening of the length in the elastic region. Under the theoretical conditions as a perfectly straight beam, constrained by ideal constraints with a perfect aligned force, the load can be increased until the bifurcation point is reached. At the bifurcation point the beam will be subjected to a transition from the fundamental deformation mode to a buckling mode, which is basically driven by the lower strain energy this mode requires. This buckling mode exhibits the characteristic half-wave deformation pattern with a stable post-buckling behaviour.

Figure 2 shows the effect of an imperfection for the beam presented in Figure 1. The geometrical imperfection, depending on how severe the imperfection is, initiates a gradual transition into the post-buckling phase up to a point where no transition is observed. The applied imperfection has a pattern similar to the first buckling mode showing an amplitude $\mu = 14.236$ mm. To demonstrate the effect of the imperfection the severity of the imperfection the amplitude μ is varied by multiplication factors: 0.25, 0.5, 1.0, 2.0 and 4.0.

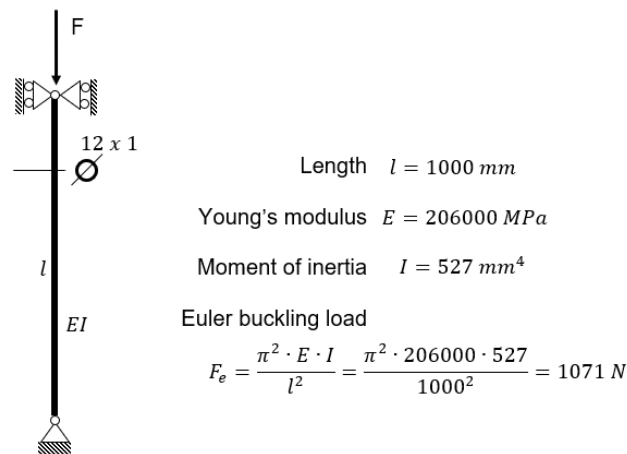


Figure 1. Euler buckling of a slender beam.

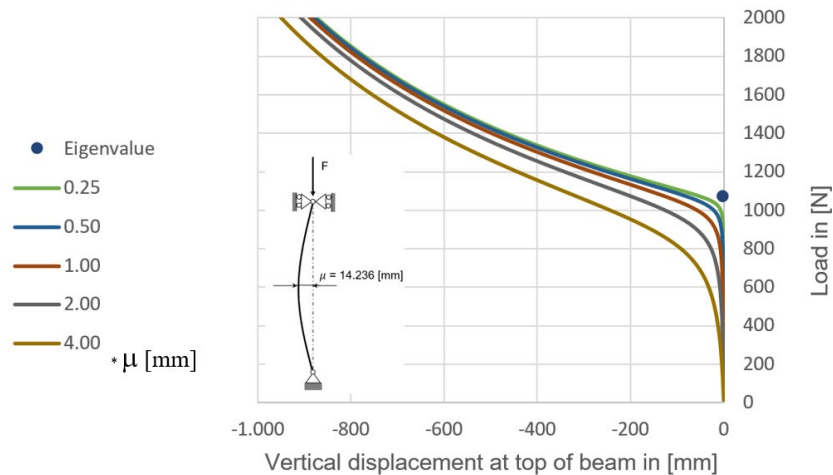


Figure 2. Deformation modes of a slender beam, imperfections with elastic material.

Figure 3 shows the load-deflection curve for the same slender beam with bi-linear material behaviour, identical applied constraints, and equivalent imperfections. The material is linear up to the yield stress $\sigma_{\text{yield}} = 355$ MPa. When the yield stress is exceeded the Young's modulus changes to a small tangent modulus $E_t = 1$ MPa. Similar to the previous example the beam will enter in a gradual manner the buckling deformation path. However, the material limit introduces a limit to the capacity of the beam, generally referred to as the limit point (according to Koiter theory the same could occur when the construction would have exhibited negative post buckling behaviour). Unlike to the post-buckling path of the slender beam with linear-elastic material, this post-buckling path is unstable and results in dynamic behaviour.

This example shows influence of geometrical imperfections and material properties. Furthermore, the plots do not demonstrate the effect of length and cross-sectional area variations. Since this beam is

relatively slender the governing failure mode is the buckling mode. However, stocky structures may fail due to yielding after progression in the fundamental deformation mode, generally referred to as collapse.

Focusing on the elastic-plastic buckling paths one can imagine a design formula based on the bifurcation point as an asymptote value. Since the aim is to prevent buckling, it is of no concern that an asymptote does not describe the post-buckling path. A proper description of the deformation can be transformed into a yield criterion.

A formulation for the vertical displacement of the beam could have the following variables:

$$u_z = c_1 \zeta \cdot \frac{F}{F_e - F}, \quad (1)$$

where F is the actual load (N), C_1 is a constant (-), ζ is the imperfection (mm) and F_e is Euler's buckling load (N).

In this paper the authors will investigate the relevance of an accurate determination of the elastic buckling load to analyse the nonlinear response following from Equation 1.

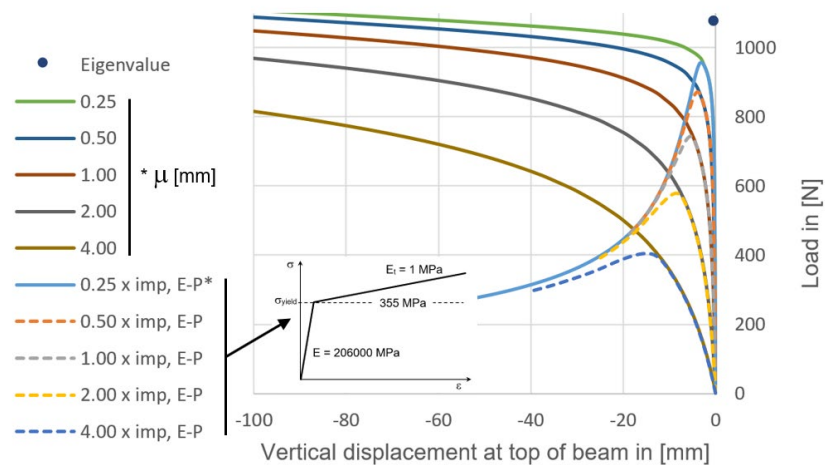


Figure 3. Deformation modes of a slender beam, with imperfections and elastic-plastic material

3 Aspects of Stiffener tripping

A submarine pressure hull consists in general of cylinders with inside or outside stiffeners. Subjected to a gradually increasing external hydrostatic pressure the cylinder will enter its fundamental deformation mode. In this mode the pressure vessel will exhibit an axisymmetric deformation of shell and stiffeners, whereby the radius of the shell midbay is smaller than the shell at the root of the web of the ring-frame due to the support of the ring-stiffeners. This support introduces a circumferential pressure and a radial load in the web plate. This load shows compression with inside and tension with outside frames. Due to balance of forces this load decreases to zero at the outer fibre of the flange. Compression in the stiffener is a destabilizing factor and could cause buckling of the web or buckling of the complete stiffener. Stiffeners on outer-stiffened cylinders experience radial tension in the web which results in a restoring moment and thus a stabilizing factor. It depends on the material properties and dimensions whether the bifurcation point of frame tripping in case of internal stiffeners is governing rather than the global or interframe buckling mode.

Wenk & Kennard [7] presented an analytical formulation for determining the axisymmetric linear elastic buckling pressure of a ring-stiffened pressure. This study was followed by the analysis for the asymmetric case [8]. The main characteristics of the derivation are summarized below:

- The cross-section of the stiffener is assumed to experience a homogeneous circumferential stress.
- The ring-stiffener is assumed to have a homogeneous radial stress through the stiffener height, i.e. from stiffener junction at the shell to the outer fibre of the flange.
- The web is assumed to be clamped at the junction of the web-root to the shell.

- The web is assumed to be a straight strip loaded by perpendicular loadings equal to the radial and circumferential loading instead of a curved plate. This simplifies the formulations since the curvature is disregarded and no polar coordinates have to be used.
- The buckling pressure is obtained by solving the determinant of coefficients in the homogeneous differential equations for a value of zero. The homogeneous equations are obtained by assuming a perfect cylinder, i.e. tilt angle equal to zero.
- The method is considered to be too extensive to present here. Therefore, a reference is made to Kennard [8] for all the specifics.

Kendrick presented a quite simplified design formulation [3], based on the conservative assumption that the web can rotate freely at the junction to the shell and does not experience the rotational stiffness of the shell.

Faulkner acknowledged the underestimation of the stiffness by a formulation that disregards the rotational stiffness. Therefore, he introduced a new formulation in which the rotational stiffness was incorporated [9].

This paper addresses a particular pressure hull design named Manatee class presented earlier by Reijmers and Stapersma [12], [13]. Figure 4 shows the overall dimensions of the pressure hull and further details are given in Table 1. For this geometry the buckling pressures following from the analytical formulations are compared with the results obtained with Finite Element Analysis. The elastic tripping pressures, determined using the analytical methods introduced above, are presented in Table 2.

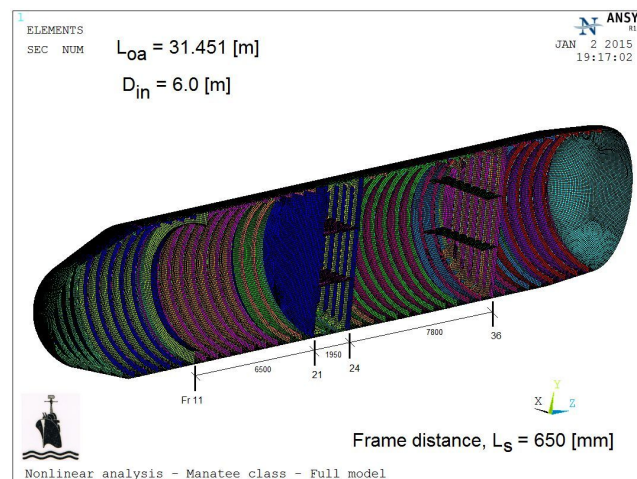


Figure 4. Pressure hull dimensions of the Manatee class.

The analytical methods above are derived in order to predict the linear elastic tripping pressure of perfect ring-stiffened pressure hulls. However, an imperfect ring-stiffener, i.e. a tilt angle in the radial-axial plane of the stiffener, causes a smooth transition from the fundamental deformation mode into the buckling deformation mode. The limit point will lie below the bifurcation point or even above, depending on the post-buckling behaviour and start of yielding. Geometry, severity of the imperfection and the material properties influence this behaviour.

Table 1. Dimensions and material properties.

Length over all	$L_{oa} = 31.451$ [m]
Inner diameter	$D_{in} = 6.0$ [m]
Frame distance	$L_s = 650$ [mm]
Hull thickness	$t = 26$ [mm]
Web plate ring frame	175×9 [mm]
Flange ring frame	120×35 [mm]
Yield stress HY 80	$\sigma_{yield} = 552$ [N/mm ²]
Young's modulus	$E = 206000$ [N/mm ²]
Poisson's ratio	$\nu = 0.30$

Table 2. Elastic tripping pressures.

Number of waves: n	Method reference		
	E.H. Kennard [8]	D. Faulkner [9]	S.B. Kendrick [3]
[-]	[MPa]	[MPa]	[MPa]
0	20.42	–	5.41
1	21.10	21.84	–
2	22.26	21.27	–
3	22.82	20.42	–
4	22.88	19.79	–
5	23.21	19.72	–
6	24.42	20.29	–
7	26.79	21.45	–

Wenk & Kennard introduced a method to predict the stresses due to an initial tilt angle for the axisymmetric case [7]. Based on these stresses the elastic buckling pressure is defined when the stresses grow to infinity. Their study was continued for the asymmetric case [8]. The stress levels in the flange according to both studies are presented in Table 3 and Table 4. These stresses are calculated at a pressure $p = 4.743$ MPa for comparison with FE analysis later on.

As mentioned in the introduction a ring-stiffened pressure hull is not only prone to frame tripping but also to global and interframe buckling. Since this paper focuses on frame tripping the methods will not be discussed on their characteristics but the results will be presented. von Mises presented a theory for the interframe buckling mode [5]. For the Manatee this theory shows a buckling pressure of $P_{E, IF} = 8.41$ MPa with 15 waves over the circumference.

The global buckling pressure following Bryant [6] shows three waves over the circumference at a pressure $P_{E, OA} = 18.11$ MPa.

 Table 3. Stress in the flange for the axisymmetric case ($n = 0$).

 Wenk & Kennard [7], Membrane stress $\sigma_{hoop} = 312.2$ MPa at $p = 4.743$ MPa

Method	First approximation [MPa]	Simplified first approximation [MPa]	Second approximation [MPa]
Amplitude on flange tip	31.4	41.3	43.5
Total stress	343.6	353.5	355.7

 Table 4. Stress in the flange for the asymmetric case ($n = 0, 3$).

 Kennard [8], Membrane stress $\sigma_{hoop} = 304.6$ MPa at $p = 4.743$ MPa

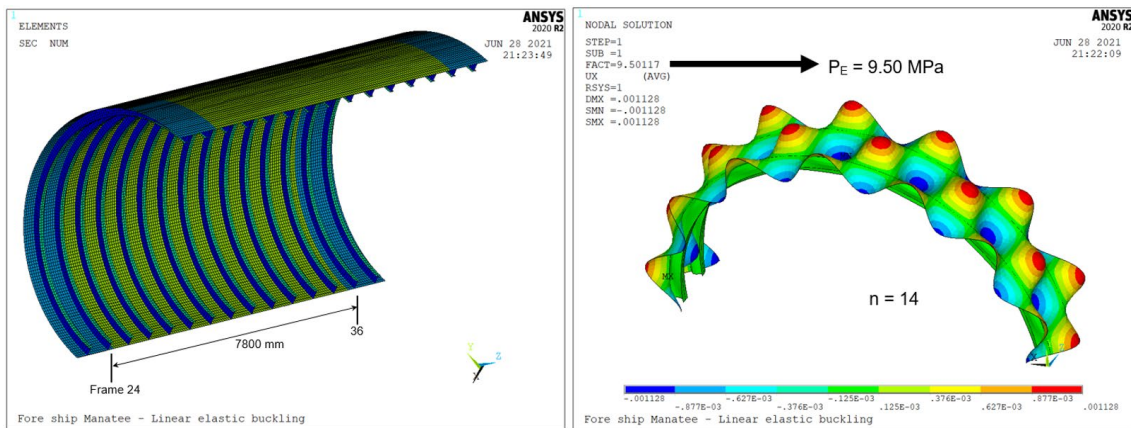
Mode	n = 0	n = 3
	Axisymmetric [MPa]	[MPa]
Amplitude on flange tip	42.7	43.8
Total stress	347.3	348.5

4 Numerical simulation

Figure 5.a shows the critical compartment of the Manatee presented in Figure 4. This is the forward compartment from frame 24 – 36. Eigenvalue analysis shows a first buckling mode addressing interframe buckling. Figure 5.b shows this mode with 14 waves over the circumference and a buckling pressure $P_E = 9.50$ MPa, which is slightly higher than the von Mises result. The analysis shows this mode for every frame bay. Furthermore, the buckling pressures for 13 to 17 waves over the circumference are of the same order. This means that a lot of eigenvalues in the lower range address interframe buckling as predicted by von Mises as well.

Stiffener tripping occurs at a higher pressure. Figure 6.a shows the mode where the complete ring frame experiences a lateral deflection ($n = 0$). This tripping mode arises at a pressure $P_E = 13.78$ MPa. This pressure is 33% lower than the tripping pressure presented by Kennard in Table 2.

At a pressure $P_E = 18.18$ MPa the first overall buckling mode is found with 3 waves over the circumference (see Figure 6.b) and this pressure matches the global buckling pressure according to Bryant.

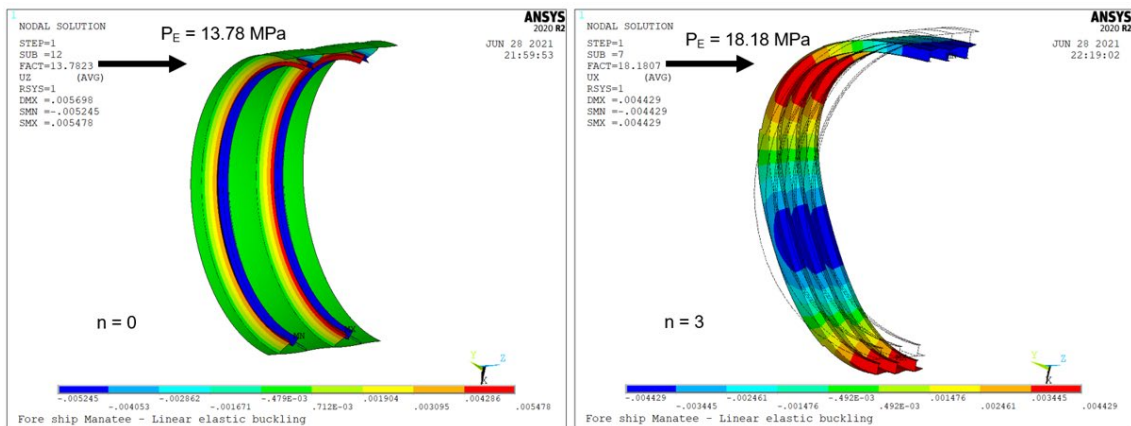


(a) Forward compartment of the Manatee (b) First buckling mode - interframe

Figure 5. Forward compartment with the lowest buckling pressure – Interframe.

In the following a nonlinear FE analysis is carried out on the forward compartment. With a focus on excessive behaviour towards elastic buckling pressures the material nonlinearity is not modelled. Stresses are not limited by plasticity and only geometrical nonlinearity is considered. To reduce runtime the model comprises a sector of 90° .

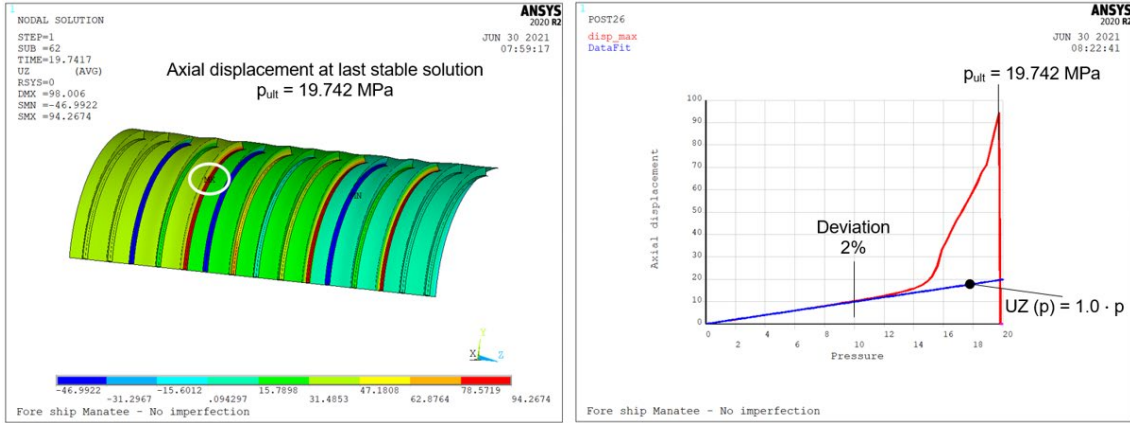
Figure 7.a presents a contour plot with axial displacement for a perfect geometry (no Out-of-Circularity and no frame tilt). The graph of the deformed model shows the location of the maximum axial displacement at the last stable solution $p_{ult} = 19.742$ MPa. Obviously, the deformation results in a lateral deflection of stiffeners which triggers the lowest tripping pressure (see Figure 6.a). Figure 7.b indicates a stable post-buckling behaviour [1]. Around a pressure of 15 MPa the axial displacement starts to deviate significantly from the linear response presented in Figure 7.b by the blue line. From 15 MPa to the ultimate pressure $p_{ult} = 19.742$ MPa the deflection shows a more or less constant slope. This analysis does not show asymptotic behaviour towards an eigenvalue and up to the tripping pressure the axial displacement is almost linear with the pressure. At a pressure $p = 10$ MPa the linear response deviates only 2% of the FE result.



(a) First stiffener tripping mode (b) First global (overall) mode

Figure 6. Stiffener tripping and global buckling.

The next analysis addresses a geometry with only Out-of-Circularity. This imperfection is modelled with 3 waves over the circumference to make it sensitive to the global buckling mode presented in Figure 6.b. The amplitude of the O-o-C is set to 0.5% of the mean radius giving 15 mm. The model is further reduced to a sector of 60° to comprise exactly a half imperfection wave with symmetry conditions.



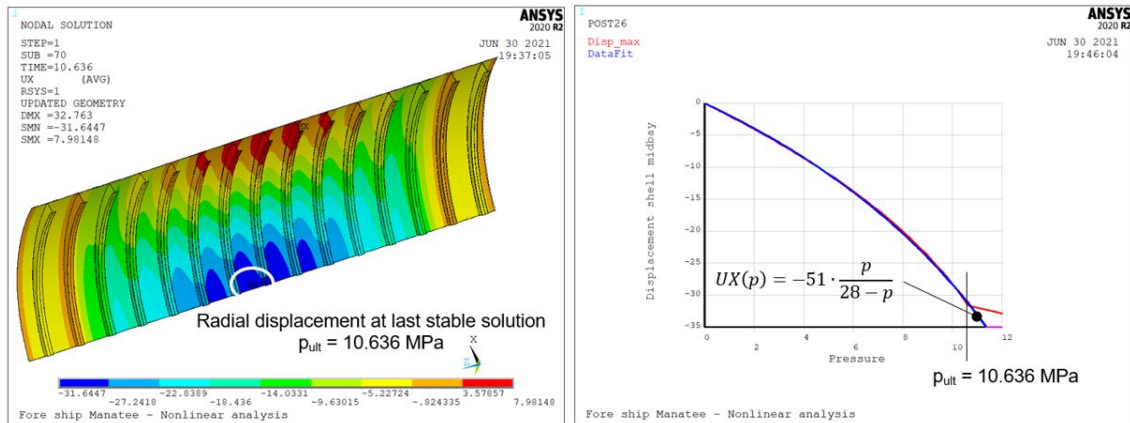
(a) Contour plot axial displacement (b) Axial displacement versus pressure

Figure 7. Geometrical non-linear response of the perfect compartment.

Figure 8.a shows a contour plot of the radial deflection and the location with the maximum inward deflection. The contour plot is given for the last stable solution $p_{ult} = 10.636$ MPa. For the location indicated in Figure 8.a, the deflection versus pressure is presented in Figure 8.b. It must be noted that Figure 8.b does not show excessive deformation at the last load step. The FE analysis stops because convergence criteria are no longer met. Although the initial O-o-C does not fit the interframe buckling mode with 14 waves over the circumference an interaction of both buckling modes cannot be excluded. The nonlinear behaviour is fitted with a hyperbolic curve with a general formulation conform Equation 1. Equation 2 describes asymptotic behaviour towards an elastic buckling pressure P_q .

$$u(p) = C \cdot \frac{p}{P_q - p} \tag{2}$$

The fit in Figure 8.b suggests an eigenvalue of 28 MPa but that is more than 50% above the calculated pressure in Figure 6.b. The response in Figure 8.b shows that there is no clear influence of the lowest global buckling pressure. As indicated in Figure 2 for the Euler beam the load can pass the bifurcation point in case of an imperfect geometry in combination with a stable post-buckling behaviour.



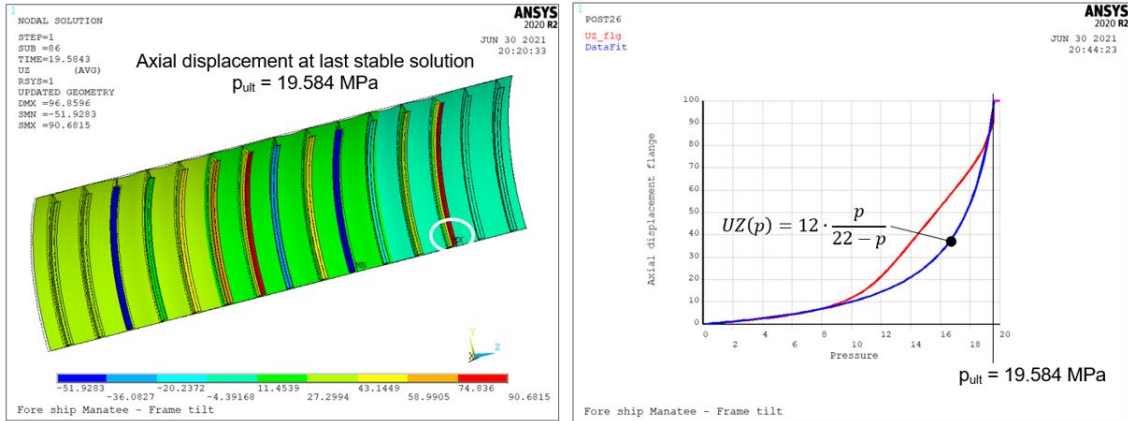
(a) Contour plot radial displacement (b) Radial displacement versus pressure

Figure 8. Geometrical non-linear response of the compartment with only O-o-C

The following analysis aims at the response of a compartment with only initial frame tilt. This imperfection is axisymmetric ($n = 0$) with a maximum tilt angle of 2° . The angle is randomly distributed over the compartment. Figure 9.a shows the axial displacement at the ultimate pressure $p_{ult} = 19.584$ MPa.

Figure 9.b presents the axial displacement versus pressure at the location indicated in Figure 9.a. Here too a fit is added conform Equation 2, but it will be clear this fit covers only the lower pressures and the ultimate pressure $p_{ult} = 19.584$ MPa. The actual displacement starts to deviate from the fit around a pressure of 10 MPa. This is lower than the tripping pressure (13.78 MPa). Furthermore, there is no

clear influence of the tripping pressure. Above 10 MPa the response increases almost linear with a higher slope towards the ultimate pressure.

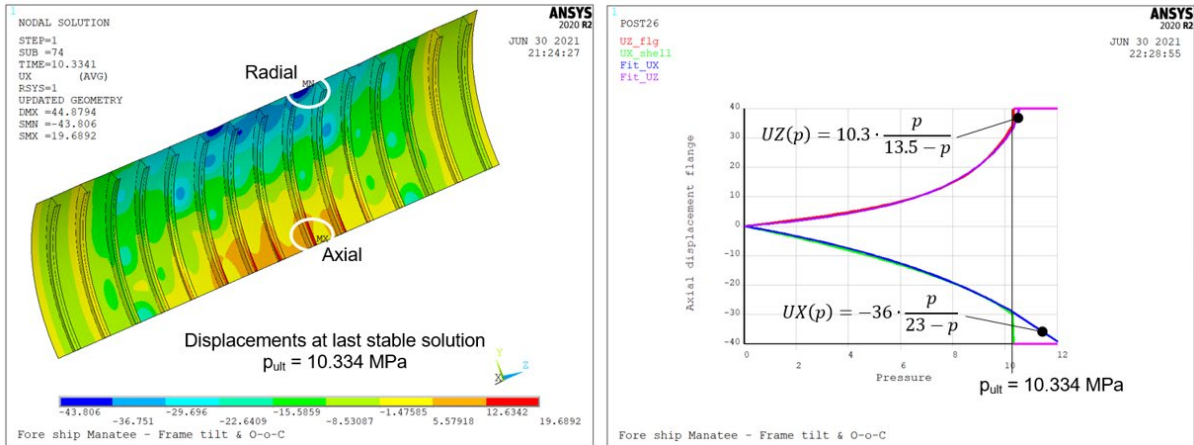


(a) Contour plot axial displacement (b) Axial displacement versus pressure

Figure 9. Geometrical nonlinear response of the compartment with only frame tilt.

Finally, the imperfections due to O-o-C and frame tilt are combined in the compartment. Figure 10.a presents the radial deflection at the ultimate pressure $p_{ult} = 10.334$ MPa. Since tilt and O-o-C are considered, two locations are indicated to assess radial displacement (addressing O-o-C) and axial displacement (for the effect of frame tilt). Figure 10.b presents these displacements versus pressure. Both graphs are fitted with a hyperbola given in Equation 2 and these fits show a better relationship with eigenvalues than found in the previous analyses.

There is a strong nonlinearity, but excessive asymptotic behaviour is cut-off by the ultimate pressure where the convergence criteria in the FE analysis are no longer met. For the axial displacement nonlinearity is driven by $P_q = 13.5$ MPa and this points at the tripping pressure $P_E = 13.78$ MPa presented in Figure 6.a. For the radial displacement the pressure $P_q = 13.5$ MPa is still 26% lower than the first global buckling pressure with three waves over the circumference ($P_E = 18.18$ MPa).



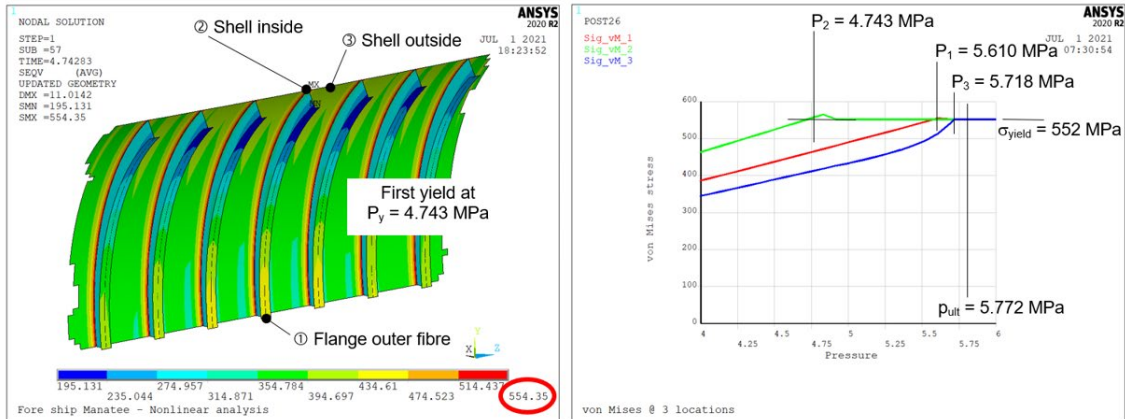
(a) Contour plot radial displacement (b) Displacements versus pressure

Figure 10. Geometrical nonlinear response with O-o-C and initial frame tilt.

5 The limiting effect of material nonlinearity

The stress levels in the analyses presented in section 4 will largely exceed the yield stress of the material under consideration. For the Manatee given in Figure 4 this material is HY80 with a yield stress $\sigma_{yield} = 552$ MPa. The applied material model is ideally elastic-plastic. This means that the material behaves linearly up to a von Mises stress equal to the yield stress. Above this stress level the Young's modulus ($E = 206000$ MPa) changes to a tangent modulus $E_t = 0.0$ MPa. With this material model the forward compartment of the Manatee is analysed. The forward compartment has an O-o-C with an amplitude of 0.5% of the mean radius and three waves over the circumference.

First yield occurs at a pressure $p_y = 4.743$ MPa and the von Mises stress at this pressure is presented in Figure 11.a. This figure also indicates the locations of interest. First yield is expected at the inside of the shell at frame location. The shell is bent over the frame and shows a high bending component in combination with axial compression. This location is numbered by ②. The location of interest is numbered by ①. The O-o-C induces bending in the frame. Location ① has an imperfection outward giving compression in the flange. In addition, the flange shows an axisymmetric compression by the hydrostatic pressure. A well accepted criterion states that yielding of the outer fibre of the flange induces collapse, however this assumption is subject to discussion [13].

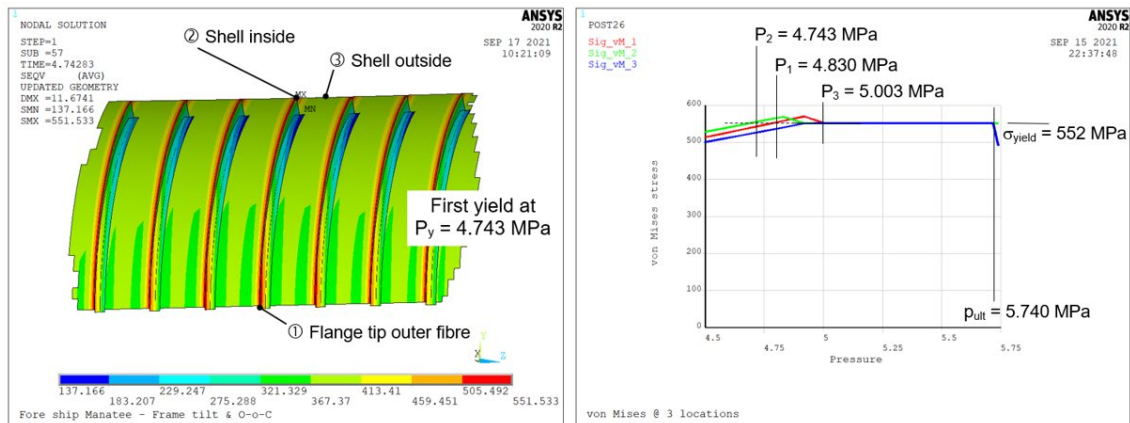


(a) von Mises stress at pressure giving first yield (b) von Mises stress versus pressure

Figure 11. Full nonlinear response in case of O-o-C only.

The shell at location ③ is also subjected to axial bending although lower than at frame location ②. On the other hand, the hoop stress midbay is higher than at frame location due to a lesser support by the ring frames. Figure 11.b shows the sequence of yielding at the three locations. Location ① yields at a pressure $P_1 = 5.610$ MPa while the ultimate pressure is $p_{ult} = 5.772$ MPa. This indicates that first yield at location ③ is closer to collapse than yielding of the outer fibre of the flange.

The analysis with material nonlinearity and imperfection by O-o-C is repeated with an additional imperfection by initial axisymmetric frame tilt ($n = 0$) with a fixed tilt angle of 2° to enable comparison with the analytical result. Figure 12 presents the results of this analysis and first yield still occurs at a pressure $p_y = 4.743$ MPa at location ②. Figure 12.b shows stresses at the three locations versus pressure and also in this case yielding of the stiffener flange does not result immediately in collapse.



(a) von Mises stress at pressure giving first yield (b) von Mises stress versus pressure

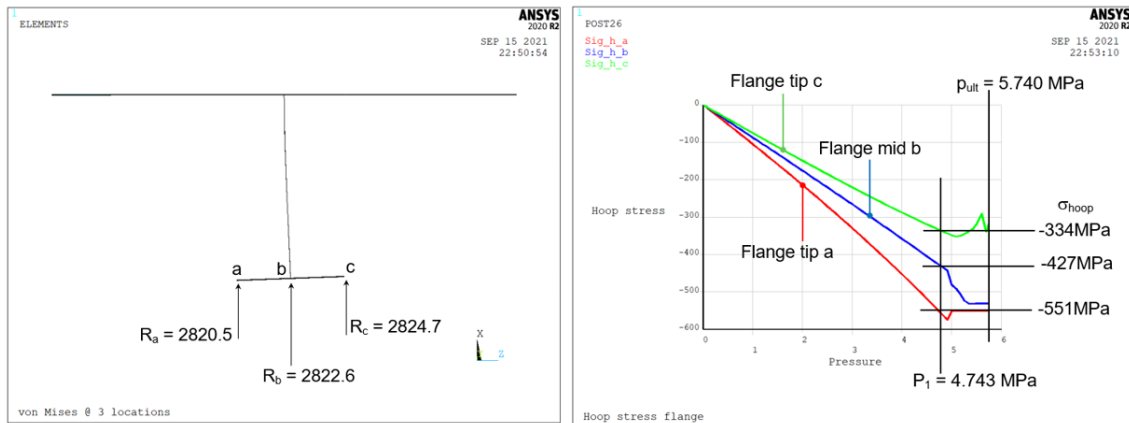
Figure 12. Full nonlinear response in case of a combination of O-o-C and frame tilt.

The shell midbay starts to yield at $P_3 = 5.003$ MPa which is significantly earlier than the pressure presented in Figure 11.b (5.718 MPa). There is still plastic reserve and finally the hull fails at a pressure $p_{ult} = 5.740$ MPa. This is only 0.6% lower than the situation with O-o-C only.

Figure 13 gives a closer look at the effect of frame tilt. Figure 13.a indicates three positions at the stiffener flange at location ① in Figure 12.a. Positions (a) and (c) show a uniaxial stress state. Axial and

radial stresses are zero and so the hoop stress equals the von Mises stress. When flange tip (a) yields the hoop stress at flange tip (c) decreases and the midpoint (b), connected to the web increases towards yield. Therefore, flange tip (a) may reach the yield stress earlier than without frame tilt, but this does not mean that the complete flange yields. At first yield the difference in hoop stress between the flange tips (a) and (c) and centre (b) is respectively 124 and 93 MPa. This is significantly higher than the amplitude presented in Table 3 and Table 1. According to Wenk and Kennard the difference between the hoop stress at the flange tip and flange centre is around 40 MPa.

It can be concluded that frame tilt has effect on the plastic behaviour of the pressure hull, but this behaviour is governed by the yield stress only. Nonlinear effects by the influence of linear elastic tripping pressures are negligible.



(a) the geometry with frame tilt (b) hoop stress at flange locations

Figure 13. The effect of frame tilt.

6 Comparison of the analytical approach and numerical simulation

The linear elastic tripping pressure predicted by Kennard and Faulkner are comparable in value, the mode numbers however are completely different, zero versus five respectively. As expected, the pressure predicted by Kendrick is considerably lower.

Table 5 presents an overview of the buckling pressures obtained with FEA and the analytical solutions. The interframe buckling pressure according to von Mises is more than 10% lower than found with FEA. This is caused by the boundary conditions in the von Mises formulation. The shell is simply supported at the frames and this neglects the stiffness provided by the frames [15]. Therefore, the real interframe buckling pressure must be higher.

The global buckling pressure according to Bryant is very close to the FEA result.

The tripping pressure is way off. The difference of 48.2% is related to Kennard but using the Faulkner formulation gives the same difference.

Table 5. Comparison FEA result and analytical solution.

Buckling pressure	FEA [MPa]	Analytical [MPa]	Reference	Difference [%]
Interframe	9.50	8.41	von Mises [5]	-11.5
Global	18.18	18.11	Bryant [6]	-0.4
Frame tripping	13.78	20.42	Kennard [8]	48.2

The geometrical nonlinear analyses hardly indicate a bifurcation point. In case of a perfect geometry the axial displacement is linear up to a pressure of 10 MPa. Nonlinearity above this pressure shows a sharp increase with a knuckle around 16 MPa. Without the foreknowledge on the actual eigenvalue solution, one could mistakenly assume, based on the envelope of the non-linear deformation path, that the bifurcation point lies near 16 MPa. However, the bifurcation point found by the FE eigenvalue solution for frame tripping is 13.78 MPa. Furthermore, the geometry has no imperfection causing magnification of the displacement. The only imperfection is imposed by the hydrostatic pressure

causing an increasing deflection from the bulkhead support to mid compartment. And this imperfection is very small.

With Out-of-Circularity the ultimate pressure is drastically lower than the buckling pressures. The imperfection is applied in the buckling mode with the lowest global buckling pressure, $n = 3$ and it is expected that the deformation is very sensitive to this mode. However, the nonlinear behaviour does not indicate asymptotic behaviour towards the buckling pressure of 18.18 MPa. It can be concluded that geometrical nonlinear analysis cannot be linked to a prominent linear elastic buckling pressure.

When material nonlinearity is considered, the nonlinear response is cut-off by plasticity. The collapse pressure is much lower than found with linear elastic material. The response shows a moderate nonlinearity and an accurate estimate of the linear elastic buckling pressure, which is 2 – 3 times higher than the collapse pressure has no effect on the collapse pressure.

The main focus of this paper lies on the elastic tripping pressure, but since the work of Wenk and Kennard is based on stress levels related to initial tilt the values presented in Table 3 and Table 4 are also compared to the numerical simulation. However, the hoop stress at the middle of the flange at the web plate connection is influenced by the O-o-C. Besides the hoop stress induced by the radial deflection the O-o-C gives a bending component which is obviously not considered by Wenk and Kennard. Nevertheless, with respect to the hoop stress in the middle ($\sigma_{\text{hoop_centre}}$) the result by Wenk and Kennard can be presented by $\sigma_{\text{hoop_centre}} \pm 43$ MPa. The FE analysis shows in Figure 13b ($\sigma_{\text{hoop_centre}} + 124$) MPa for flange tip a and ($\sigma_{\text{hoop_centre}} - 93$) MPa for flange tip c. This means that the analytical solution is a factor two to three lower than the result by numerical simulation. It must be noted that the comparison is based on one geometry only, namely the Manatee class. An extension to other geometries is imperative to achieve more insight in the bias of the stress levels. The numerical analysis shows in Figure 13.b for the hoop stresses a nonlinear increase of the flange tips. The analytical solution is based on a linear approach.

7 Conclusion

The main focus of this paper lies on the relevance of buckling pressures and lateral buckling or stiffener tripping in particular. The analytical solutions for the tripping pressures are overestimated by more than 40%, while the global buckling pressure shows a good match. However, when geometrical nonlinear analyses are carried out the influence of buckling pressures is not clearly visible. This is explained by the basic analysis of an Euler beam. With imperfection this beam shows a stable post-buckling behaviour, and the presence of a bifurcation point disappears. The necessity of an accurate calculation of this eigenvalue disappears also.

When material nonlinearity is considered the collapse pressures are much lower compared to the elastic buckling pressures. Nevertheless, stresses increase nonlinear with the pressure and to cover this nonlinear behaviour design methods are often based on an asymptotic increase towards a buckling pressure, in particular for global buckling but not for tripping. It is found that this nonlinearity is relatively small in the pressure range towards plastic collapse but nevertheless should not be ignored for global collapse.

Although the influence of an initial tilt angle on the collapse pressure cannot be neglected it is small compared to the influence of Out-of-Circularity. This reduces the need for an accurate tripping analysis but an analytical stress solution that is off by a factor two to three as found in this paper seems unsatisfactory. Therefore, improvement of the analytical stress solution is recommended. So, with respect to initial tilt and tripping pressures it is recommended to focus on stress levels instead of eigenvalues.

8 References

- [1] Hutchinson, J. and Koiter, W. T., "Postbuckling theory", Journal of Mathematics and Physics, 1968, Vol. 47.
- [2] Budiansky, B. and Amazigo, J. C., "Initial post-buckling behavior of cylindrical shells under external pressure", Journal of Mathematics and Physics, 1968, Vol.47.
- [3] Kendrick, S. B., "The stress analysis of pressure vessels and pressure vessel components", First edition, Pergamon press, 1970, Chapter 9.

- [4] von Mises, R., "Der kritische Aussendruck zylindrischer Rohre", Zeitschrift Des Vereines Deutscher Ingenieure, 1914, Band 58, Nr. 19.
- [5] von Mises, R., "The critical external pressure of cylindrical tubes under uniform radial and axial load", United States Experimental Model Basin, 1933. Translation report 366.
- [6] Bryant, A. R., "Hydrostatic pressure buckling of a ring-stiffened tube", Naval Construction Research Establishment, 1954, NCRE report 306.
- [7] Wenk, E., & Kennard, E. H., "The weakening effect of initial tilt and lateral buckling of ring stiffeners on cylindrical pressure vessels", David Tylor Model Basin, 1956, DTMB report 1073.
- [8] Kennard, E. H., "Tripping of T-shaped Stiffening Rings on Cylinders under External Pressure", David Tylor Model Basin, 1959, DTMB report 1079.
- [9] Faulkner, D., "Application of reliability theory in submarines design", presented at Advances in Marine Structures – 2, Dunfermline, 1991, page 566.
- [10] Shiomitsu, D. and Yanagihara, D., "Elastic local shell and stiffener-tripping buckling strength of ring-stiffened cylindrical shells under external pressure", Thin-Walled Structures 148, 2020, <https://doi.org/10.1016/j.tws.2020.106622>
- [11] Shiomitsu, D., and Yanagihara, D., "Estimation of ultimate strength of ring-stiffened cylindrical shells under external pressure with local shell buckling or torsional buckling of stiffeners", Thin-Walled Structures 161, 2021, <https://doi.org/10.1016/j.tws.2020.107416>
- [12] Reijmers, J. J., "Reliability based pressure hull design", presented at NAFEMS World Congress, San Diego, 2015.
- [13] Reijmers, J. J., and Stapersma, D., "Uncertainty quantification with respect to global collapse of submarine pressure hulls compared to interframe collapse", presented at NAFEMS World Congress, Stockholm, 2017.
- [14] Germanischer Lloyd, "III Rules for Classification and Construction, Part 1 Underwater Technology", Edition 1998, Chapter 2 Submersibles.
- [15] Reijmers, J. J., "The job and the tools", NAFEMS Benchmark Magazine, October 2007.